Journal of Environmental Economics & Chemical Processes (JEECP)

https://doi.org/10.22034/jeecp.2026.2089306.1030

Journal Homepage: WWW.JEECPJournal.com

Journal of Environmental Economics & Chemical Processes (JEECP)

ORIGINAL RESEARCH PAPER

Metal-Dependent Oxidative Desulfurization of Real Gas Condensate over Modified Iranian Kaolin-Supported Catalysts

Tahereh Mojtahed [a]; Fereshteh Abbasi Oghani [b]; Alimorad Rashidi [c, *]; Kimia Shahbazi [d]

[a] *Department of Chemistry, Science and Research Branch, Islamic Azad University, Tehran, Iran.*
[b] *Department of Chemical Engineering, Science and Research Branch, Islamic Azad University, Tehran, Iran.*
[c] *Nanotechnology Research Center, Research Institute of Petroleum Industry (RIPI), Tehran, Iran.*
[d] *Department of Chemical Technologies, Iranian Research Organization for Science and Technology (IROST), Tehran, Iran.*

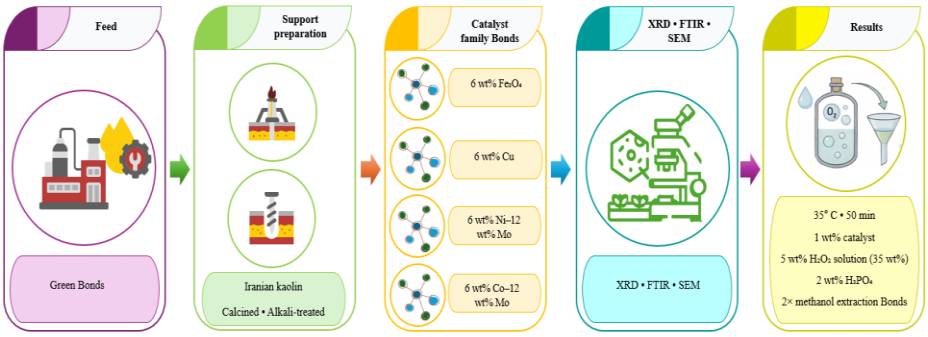
P A P E R I N F O

Paper history:
Received: 08/07/2026
Revised: 10/04/2026
Accepted in revised form: 10/14/2026
Published: 03/30/2027

***Keywords*:**
Natural Iranian Kaolin;
Oxidative Desulfurization;
Real gas Condensate;
Fe_3O_4–Kaolin;
Heterogeneous Catalyst;
Hydrogen Peroxide.

A B S T R A C T

Natural Iranian kaolin was calcined, alkaline-treated, and used as a common aluminosilicate support for Fe_3O_4–kaolin, Cu–kaolin, NiMo–kaolin, and CoMo–kaolin catalysts with nominal loadings of 6 wt% Fe_3O_4, 6 wt% Cu, 6 wt% Ni–12 wt% Mo, and 6 wt% Co–12 wt% Mo, respectively. X-ray diffraction, Fourier-transform infrared spectroscopy, and scanning electron microscopy were used to compare the crystalline structure, bonding environment, and morphology of the prepared materials. The XRD patterns retained the disordered kaolin-derived background and residual mineral reflections while showing distinct metal-dependent crystalline contributions. Catalytic performance was evaluated using a real gas-condensate feed containing 1500 ppm total sulfur. Oxidation was conducted at 35 °C for 50 min in a closed batch reactor using 1 wt% catalyst, 5 wt% of a 35 wt% H_2O_2 solution, and 2 wt% H_3PO_4, followed by two successive methanol extractions. Metal-free modified kaolin decreased the sulfur concentration to 840 ppm, corresponding to 44.00% overall removal. Residual sulfur concentrations of 136, 770, 555, and 528 ppm were obtained with Fe_3O_4–kaolin, Cu–kaolin, NiMo–kaolin, and CoMo–kaolin, respectively. Fe_3O_4–kaolin provided the highest overall removal efficiency, 90.93%, under the selected oxidation–extraction conditions.



1. Introduction

Sulfur-containing compounds in petroleum-derived fuels contribute to equipment corrosion, catalyst deactivation, and sulfur oxide emissions. Hydrodesulfurization remains the principal industrial treatment, but its hydrogen demand and severe operating conditions have encouraged the development of complementary routes for sulfur species that are less reactive toward conventional hydrotreating. Oxidative desulfurization (ODS) converts organosulfur compounds into more polar sulfoxides and sulfones, which can subsequently be removed by extraction or adsorption. Applications to model fuels and real gas-condensate streams have established the relevance of this approach for compositionally complex petroleum feeds [1–3]. The effectiveness of ODS is governed by oxidant activation, catalyst composition, contact between the hydrocarbon and oxidizing phases, and the subsequent separation of oxidized sulfur products. Hydrogen peroxide is commonly selected as the oxygen donor because it operates under comparatively mild conditions and produces water as the principal reduction product. In biphasic systems, agitation promotes interfacial mass transfer during oxidation, while polar solvents such as methanol remove sulfoxides and sulfones from the treated hydrocarbon phase [4, 5]. Natural aluminosilicates offer abundant and chemically adaptable supports for heterogeneous catalysts. Calcination of kaolinite removes structural hydroxyl groups and generates a disordered metakaolin-like matrix; subsequent alkaline treatment modifies reactive Si–O–Al and Si–O–Si environments through partial dissolution and reorganization.

* Corresponding Author: Alimorad Rashidi
E-mail address: rashidiam@gmail.com
ISSN: 3116-0050
URL: https://www.jeecpjournal.com/article_736319.html

Please cite this article as: T. Mojtahed, F. Abbasi Oghani, A. M. Rashidi, & K. Shahbazi, *Journal of Enviromental Economics & Chemical Processes (JEECP)*, 2027, *4*(1), 9-14. https://org.org/10.22034/jeecp.2026.2089306.1030

/© 2027 The Author(s). Published by Power of New Vision Movement Institute.

Accessory quartz may remain crystalline after these treatments. Modified kaolin has consequently been investigated as a carrier for ODS-active oxides and in catalytic treatment of sour petroleum fractions [6, 7].

Metal identity influences the interaction with oxidants and the overall ODS response. Iron- and copper-containing catalysts have been investigated in peroxide-based ODS [8–10], while a peroxo-mediated pathway has been proposed for supported molybdenum species in an H_2O_2 system [23]. Supported cobalt and nickel molybdates have also been examined as ODS catalysts [11, 12].

These studies motivate comparing different metal-containing formulations, although the response depends on phase composition, dispersion, support interaction, and operating conditions. This study compares Fe_3O_4–kaolin, Cu–kaolin, NiMo–kaolin, and CoMo–kaolin prepared on the same calcined and NaOH-modified Iranian kaolin support. Their crystalline structures, bonding environments, surface morphologies, and sulfur-removal performances were examined under a common preparation and reaction protocol. The comparison was designed to clarify how the incorporated metal system altered the kaolin-derived material and affected the overall oxidative desulfurization of a real gas-condensate feed..

2. Method

2.1. Methodology

Natural Iranian kaolin was supplied by Parsian Mineral Chemical Company, Iran. Industrial-grade NaOH flakes were used for alkaline modification. Commercial Fe_3O_4 powder, $Cu(NO_3)_2{\cdot}3H_2O$, $Ni(NO_3)_2{\cdot}6H_2O$, $Co(NO_3)_2{\cdot}6H_2O$, and $(NH_4)_6Mo_7O_{24}{\cdot}4H_2O$ were supplied by Merck and used as received. Hydrogen peroxide solution (35 wt%), industrial-grade H_3PO_4, industrial-grade methanol, and distilled water were used without further purification.

2.2. Support Modification and Preparation of Metal-Loaded Materials

Natural kaolin was first calcined at 550 °C for 6 h. The calcined material was treated with NaOH in an aqueous medium at a kaolin-to-NaOH mass ratio of 1:3, with stirring at approximately 400 rpm for 6 h.

The alkaline-treated solid was recovered by centrifugation, washed repeatedly with portions of distilled water to remove readily soluble alkaline residues, and allowed to dry overnight. A second calcination at 550 °C for 6 h produced the modified kaolin support. The metal-loaded materials were prepared by aqueous wet impregnation or dispersion-assisted deposition. For NiMo–kaolin and CoMo–kaolin, the nickel or cobalt nitrate precursor was dissolved in water, H_3PO_4 was added, and the aqueous ammonium heptamolybdate solution was then introduced.

The modified support was subsequently added to this combined precursor solution. For Cu–kaolin, copper nitrate was dissolved in water and the solution was acidified with H_3PO_4 before addition of the support. For Fe_3O_4–kaolin, commercial Fe_3O_4 powder was dispersed in water, H_3PO_4 was added, and the modified support was introduced. Each resulting suspension was stirred for 1 h, dried at 100 °C for 12 h, and calcined at 550 °C for 6 h.

Table 1. Nominal compositions and thermal treatment of the prepared materials

Catalyst	Nominal loading	Post-loading treatment
Fe_3O_4–kaolin	6 wt% Fe_3O_4	100° C, 12 h; calcination at 550 °C, 6 h
Cu–kaolin	6 wt% Cu	100° C, 12 h; calcination at 550 °C, 6 h
NiMo–kaolin	6 wt% Ni + 12 wt% Mo	100° C, 12 h; calcination at 550 °C, 6 h
CoMo–kaolin	6 wt% Co + 12 wt% Mo	100° C, 12 h; calcination at 550 °C, 6 h

All nominal loadings in Table 1 were calculated relative to the dry mass of the modified support. The Cu, Ni, Co, and Mo loadings denote metal-equivalent masses supplied by their precursors, whereas the Fe_3O_4 loading denotes the mass of commercial oxide powder. These are nominal preparation ratios rather than experimentally determined metal contents.

2.3. Oxidative Desulfurization and Extraction

A real industrial gas-condensate feed containing 1500 ppm total sulfur was used in the ODS experiments. The metal-free modified kaolin support and each metal-loaded catalyst were evaluated separately using 130 mL of feed in a closed metallic batch reactor. Catalytic tests were performed in three independent ODS reactions for each material. The catalyst was added first at 1 wt%, followed by 5 wt% of a 35 wt% H_2O_2 solution and 2 wt% H_3PO_4; all three additions were specified relative to the initial feed mass. The reactor was maintained at 35 °C in a water bath, and oxidation was continued for 50 min under continuous stirring. This duration refers to oxidation and excludes the subsequent separation and extraction steps. The feed properties are summarized in Table 2. After oxidation, the catalyst was removed by centrifugation. The liquid was transferred to a decanter, the aqueous phase was removed, and the recovered hydrocarbon-rich phase was extracted twice with fresh methanol. Each extraction used 130 mL of methanol, corresponding to a methanol-to-initial-feed volume ratio of 1:1. The phases were mixed for 30 min and then allowed to separate for 30 min. The methanol-rich phase was removed before the next extraction. Total sulfur in the untreated feed and the hydrocarbon phase recovered after the second extraction was determined by energy-dispersive X-ray fluorescence using a HORIBA SLFA-6000 sulfur-in-oil analyzer (HORIBA, Japan) in accordance with ASTM D4294-24 [13]. Each feed and product sample was measured three times by XRF, giving three analytical readings per sample (n = 3). The reported sulfur concentrations are the arithmetic means of these readings; the individual readings are provided in Table S1. Figure 1 illustrates the oxidation, separation, and two-stage methanol extraction sequence



Figure 1. Illustrated workflow of the oxidation–extraction procedure and total sulfur analysis. Aqueous-phase separation is followed by two successive extractions with fresh methanol

Table 2. Reported properties of the real gas-condensate feed.

Property	Unit	Value
Density at 15 °C	g cm^{-3}	0.750
API gravity	°API	57.2
Initial total sulfur	ppm	1500
Equivalent total sulfur	wt%	0.150

2.4. Physicochemical, Structural, and Morphological Characterization

Powder X-ray diffraction patterns were recorded using a Bruker AXS D8 Advance diffractometer. FTIR spectra were collected with a PerkinElmer Spectrum 65 spectrometer in the mid-infrared region. Surface morphology was examined using an FEI Quantum 2000 scanning electron microscope. Phase assignments were based on peak positions and the overall diffraction sequence; Rietveld refinement and quantitative phase analysis were not performed.

2.5. Calculations

Overall sulfur removal after the combined oxidation and extraction sequence was calculated as:

$$\textit{Sulfur removal (\%)} = [(C_{o,S} - C_{f,S}) / C_{o,S}] \times 100$$

where C_o,S and C_f,S are the initial and residual total sulfur concentrations, respectively. For a 100 g feed basis, 1500 ppm sulfur corresponds to 0.15 g or

4.68 mmol elemental sulfur. Five grams of 35 wt% H_2O_2 solution contains 1.75 g or approximately 51.4 mmol H_2O_2, giving an initial H_2O_2-to-sulfur molar ratio of approximately 11.0. This nominal ratio exceeds the stoichiometric ratio of 2 for oxidation of a divalent organosulfur compound to the corresponding sulfone [14].

Sample standard deviations were calculated using the n − 1 denominator for three XRF readings per sample (n = 3). Sulfur removal was calculated from the unrounded mean feed and product concentrations. The SDs describe within-sample analytical variability and do not estimate variability between independent ODS reactions. The Type A standard uncertainty of each mean, calculated as SD/√3, is reported in Table S1. This repeatability estimate excludes calibration, bias, matrix effects, and between-reaction variability.

3. Results and Discussion

3.1. X-ray Diffraction (XRD)

Figure 2 compares the XRD patterns of modified kaolin and the four metal-loaded materials. The modified support displayed a broad diffuse contribution between approximately 15 and 35° 2θ together with a dominant sharp reflection near 26.6°. The diffuse component reflects the loss of long-range kaolinite order during calcination and alkaline treatment, whereas the intense reflection near 26.6° is assigned mainly to residual quartz in the natural mineral [15, 16].

The support-related quartz reflection remained visible after metal loading, and each formulation showed additional reflections. Fe_3O_4–kaolin displayed iron-oxide-related features across the intermediate- and high-angle regions. Cu–kaolin exhibited a group of peaks around 32–39° and additional reflections at higher angles, consistent with CuO-containing kaolin composites [16].

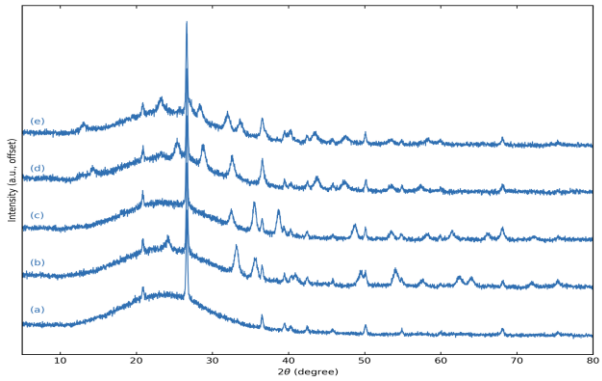


Figure 2. XRD patterns of (a) NaOH-modified calcined kaolin, (b) Fe_3O_4–kaolin, (c) Cu–kaolin, (d) NiMo–kaolin, and (e) CoMo–kaolin

NiMo–kaolin and CoMo–kaolin produced more complex patterns, with multiple reflections superimposed on the kaolin-derived background. Their different peak positions and relative intensities indicate distinct crystalline contributions after the final thermal treatment. Mixed molybdate/oxide environments are a possible interpretation of these patterns [11, 12]; individual phases were not quantified.

The XRD results show that the common modified-kaolin matrix was retained in all samples while the loaded metal systems generated distinguishable crystalline contributions. Phase identification was therefore used qualitatively to compare the prepared catalysts.

3.2. FTIR Spectroscopy

Figure 3 compares the FTIR spectra of the four metal-loaded materials. Broad O–H stretching bands occur at 3460.76–3521.31 cm^{-1}, and absorptions at 1634.20–1638.88 cm^{-1} are attributed mainly to H–O–H bending of adsorbed water. Distinct kaolinite hydroxyl bands near 3695–3620 cm^{-1} and the Al–OH deformation near 912 cm^{-1} are not resolved in these spectra, consistent with thermal dehydroxylation and subsequent alkaline modification [16-19]. The spectra do not quantify the extent of dehydroxylation. The narrow feature at 2356.89 cm^{-1} in Fe_3O_4–kaolin is compatible with atmospheric CO_2.

The principal Si–O–T stretching features, where T denotes Si or Al, occur at 1084.16, 1092.46, 995.72, and 1090.81 cm^{-1} for Fe_3O_4–kaolin, Cu–kaolin, CoMo–kaolin, and NiMo–kaolin, respectively. Cu–kaolin and NiMo–kaolin show shoulders at 1226.93 and 1214.79 cm^{-1}, while CoMo–kaolin has an additional feature at 1102.75 cm^{-1}. These features fall within the broad aluminosilicate stretching envelope. Bands at 800.43, 798.28, and 797.89 cm^{-1} in Fe_3O_4–kaolin, Cu–kaolin, and NiMo–kaolin can include symmetric silicate vibrations, residual-quartz contributions, and Al–O bending [16, 18]. The different envelopes describe the local bonding environments of the final formulations; they do not quantify metal loading or dispersion.

Al–O–Si and Si–O–Si framework deformation modes contribute to the lower-wavenumber region around 450–550 cm^{-1} [16]. Fe_3O_4–kaolin exhibits bands at 552.99 and 456.59 cm^{-1}. An Fe–O contribution may overlap with the support vibrations in this region, but a separate iron–oxygen band cannot be assigned unambiguously from this spectrum [17]. Cu–kaolin and NiMo–kaolin show features at 553.15/455.59 and 553.02/453.73 cm^{-1}, respectively. Their similar positions illustrate the overlap of framework and possible metal–oxygen contributions. CoMo–kaolin exhibits additional bands at 690.05, 626.37, 575.90, 509.15, and 462.31 cm^{-1}. Metal–oxygen modes, including possible Co–O–Mo and Mo–O contributions, may overlap with the aluminosilicate vibrations [20]. These bands are not used as unique phase identifiers.

Nickel molybdate reference materials show lower-frequency metal–oxygen vibrations, with band positions differing between preparation routes [21]. Distinct nickel molybdate hydrate compounds also have different structural and spectroscopic signatures [22]. These reference spectra provide context for overlapping Mo-containing vibrations; they do not establish a particular molybdate phase in the calcined kaolin composite.

The absorption at 1427.69 cm^{-1} in CoMo–kaolin is compatible with carbonate species associated with alkaline treatment and exposure to atmospheric CO_2 [18]. Overall, the Si–O and Al–O-related features characterize the modified aluminosilicate framework, while the lower-wavenumber region provides context for possible metal–oxygen contributions. Fe_3O_4–kaolin gave the highest sulfur removal within the tested series, but the FTIR spectra do not establish which sites governed that response. Iron oxidation states, active-site concentrations, and peroxide-activation pathways cannot be determined from these band positions [23, 24]

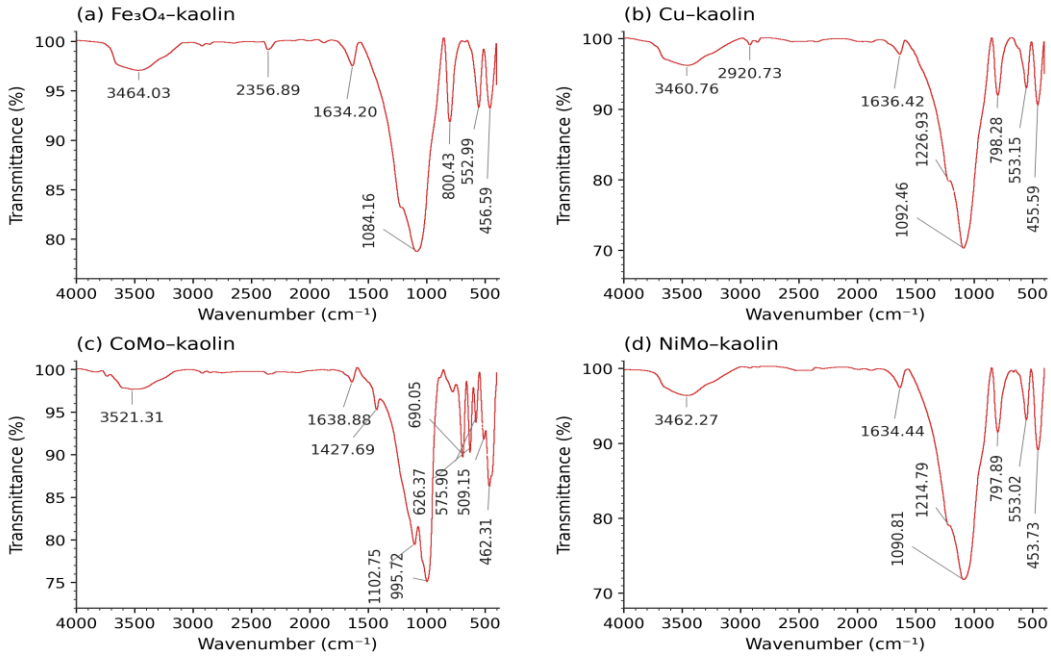


Figure 3. FTIR spectra of (a) Fe_3O_4–kaolin, (b) Cu–kaolin, (c) CoMo–kaolin, and (d) NiMo–kaolin

3.3. Surface Morphology

The SEM micrographs in Figure 4 show heterogeneous aggregates containing plate-like kaolin-derived fragments and finer surface particulates. Fractured edges and rough surfaces were visible in the prepared materials, and the extent of granular coverage differed among the four formulations.

Fe_3O_4–kaolin displayed rough nodular aggregates and locally cauliflower-like clusters assembled from smaller particles. Plate-like regions of the support remained visible between the granular domains, consistent with morphologies reported for iron-oxide/kaolin composites [17]. Cu–kaolin preserved the clearest lamellar features and showed more localized deposits along platelet surfaces and edges [16].

CoMo–kaolin and NiMo–kaolin exhibited more extensive particulate coverage and multiscale agglomeration. The CoMo formulation showed interconnected clusters over irregular support fragments, whereas the NiMo sample contained denser rounded aggregates that partly masked the platelets. These images show differences in the final morphology; the chemical composition of individual deposits was not resolved by SEM.

The SEM comparison distinguishes external morphology and apparent surface coverage. Visible clusters were treated as morphological aggregates, and their dimensions were not interpreted as crystallite sizes. Because the panels were recorded at different nominal magnifications, the comparison is qualitative and does not support direct particle-size quantification.

3.4. Overall Sulfur Removal

Table 3 summarizes the mean residual total sulfur concentrations and their analytical SDs after oxidation and two-stage methanol extraction. Metal-free modified kaolin decreased sulfur from 1500 to 840 ppm, corresponding to 44.00% overall removal. Fe_3O_4–kaolin decreased the residual sulfur concentration to 136 ppm and achieved 90.93% removal. CoMo–kaolin and NiMo–kaolin produced residual concentrations of 528 and 555 ppm, corresponding to 64.80 and 63.00% removal, respectively, while Cu–kaolin produced 770 ppm residual sulfur and 48.67% removal.

The overall performance order was Fe_3O_4–kaolin > CoMo–kaolin > NiMo–kaolin > Cu–kaolin > modified kaolin. Relative to the metal-free support, the increase in removal efficiency was 46.93 percentage points for Fe_3O_4–kaolin, 20.80 for CoMo–kaolin, 19.00 for NiMo–kaolin, and 4.67 for Cu–kaolin.

Because methanol extraction followed the oxidation stage, the reported values describe overall sulfur removal across the complete oxidation–extraction sequence.

Table 3. Mean total sulfur concentrations and overall removal after oxidation and methanol extraction.

Material	Feed sulfur (ppm)	Product sulfur (ppm)	Removal (%)
Modified kaolin	1500.0 ± 3.6	840.0 ± 2.6	44.00
Fe_3O_4–kaolin	1500.0 ± 3.6	136.0 ± 1.0	90.93
Cu–kaolin	1500.0 ± 3.6	770.0 ± 1.7	48.67
NiMo–kaolin	1500.0 ± 3.6	555.0 ± 1.0	63.00
CoMo–kaolin	1500.0 ± 3.6	528.0 ± 5.6	64.80

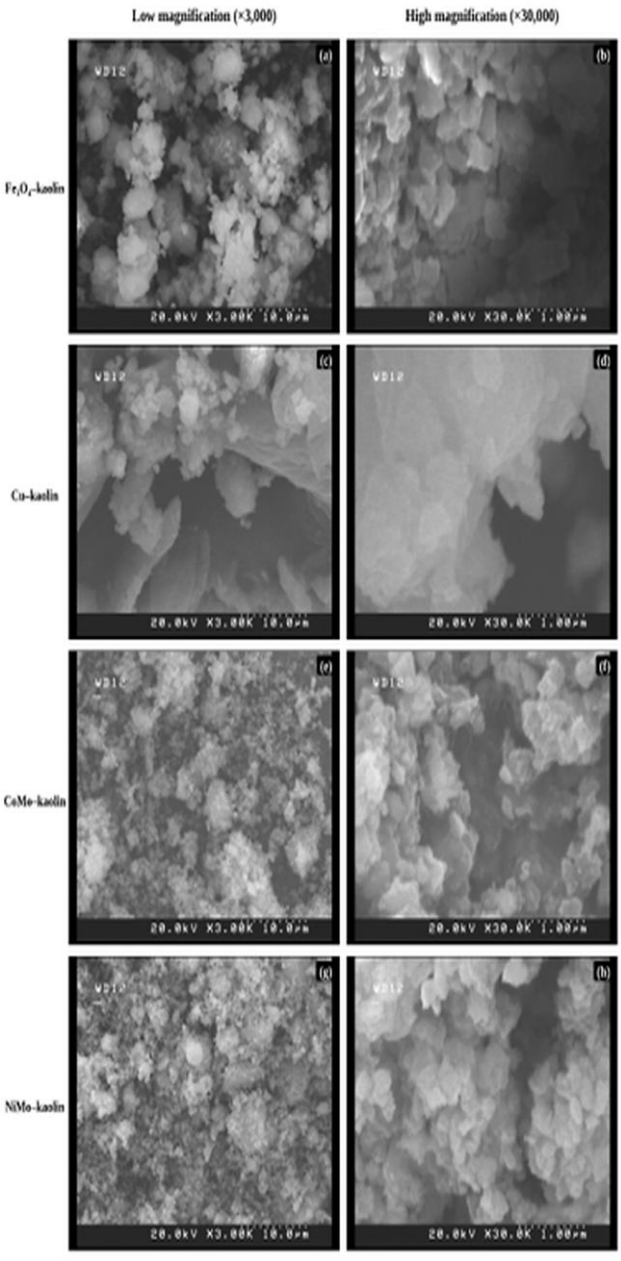
Sulfur concentrations are means ± sample SDs of three XRF readings per sample (n = 3). SD describes within-sample analytical variability. Overall removal was calculated using the common mean feed concentration of 1500 ppm. Calculations retained full precision; SDs are displayed with two significant figures. Individual readings and statistical definitions are provided in Table S1. Independent-reaction variability is not estimated by these SDs.

3.5. Interpretation of the Metal-Dependent Response

The metal-free support gave 44.00% overall sulfur removal under the same oxidation–extraction conditions used for the metal-containing formulations, providing a reference for their comparison. The higher overall removal obtained with the metal-containing formulations shows differences in the performance of the prepared materials. This comparison does not isolate the individual contributions of adsorption, catalytic oxidation, and methanol extraction.

Fe_3O_4–kaolin gave the highest overall sulfur removal and displayed a rough, heterogeneous surface with additional iron-oxide-related diffraction features. Peroxide-driven ODS has been reported for supported iron-containing catalysts [9]. Fe^{2+}/Fe^{3+} redox cycling is a possible interpretation of the response, but the iron oxidation-state distribution and peroxide-activation pathway were not directly measured in this study. CoMo–kaolin and NiMo–kaolin showed intermediate removal efficiencies and multiscale aggregation. Their diffraction patterns contained metal-dependent crystalline contributions, while their FTIR spectra were dominated by aluminosilicate bands with possible overlapping metal–oxygen modes. Supported cobalt and nickel molybdates have been evaluated in ODS systems [11, 12]. Molybdenum peroxo species are possible intermediates in the present H_2O_2 system: this pathway has been considered for Mo/Al_2O_3 with H_2O_2 [23], but reactive intermediates were not measured here.

Cu–kaolin gave the lowest overall removal among the metal-containing formulations and exceeded the metal-free support by 4.67 percentage points. Its XRD profile contained copper-oxide-related crystalline features, while SEM showed exposed plate-like support regions and localized particulate deposits. Oxidation state, dispersion, and metal–support interaction have been discussed as factors in Cu-based ODS performance [8, 10]. Their separate contributions were not determined by the present characterization.



3.6. Comparison with Reported ODS Systems

Fe_3O_4–kaolin achieved 90.93% overall sulfur removal from a real gas-condensate feed using oxidation at 35 °C for 50 min followed by two methanol extractions. A homogeneous $H_2SO_4/HNO_3/NO_2$ system achieved 95.56% removal from real sour gas condensate [2,25]. Porous MoS_2 provided 93.44% removal at 75 °C over 2 h [1], while V_2O_5/mesoporous kaolin produced near-complete dibenzothiophene conversion in a model fuel at 60 °C [6]. The present study demonstrates substantial overall removal from a real feed at a lower oxidation temperature than these two heterogeneous examples. Differences in feed composition and processing conditions prevent a quantitative ranking of the catalysts across studies. Table 4 compares the operating conditions and reported outcomes of these studies[26].

Table 4. Contextual comparison with selected ODS studies

System and feed	Main conditions	Reported sulfur response
Fe_3O_4–kaolin; real gas condensate (present study)	35 °C; 50 min oxidation; 1 wt% solid; 5 wt% of 35 wt% H_2O_2; 2 wt% H_3PO_4; two methanol extractions (30 min mixing + 30 min phase separation per stage)	90.93% overall removal; 1500 to 136 ppm
$H_2SO_4/HNO_3/NO_2$; real sour gas condensate [2]	Optimized homogeneous oxidation	95.56% removal
2D porous MoS_2; sour gas condensate [1]	75 °C; 2 h; 0.2 wt% catalyst; 3 wt% H_2O_2	93.44% removal
V_2O_5/mesoporous kaolin; model DBT fuel [6]	60 °C; 10 min; O/S = 4	Near-complete DBT conversion

The reported studies provide context rather than a direct catalyst ranking. Feed composition, sulfur speciation, oxidant dosage, and separation procedures vary among them. The 50 min reported for the present study is the oxidation time; each subsequent methanol extraction involved 30 min of mixing and 30 min of phase separation.

The characterization and performance results have several limitations. The reported loadings are nominal preparation ratios; actual metal contents, specific surface area, pore structure, quantitative metal dispersion, and surface oxidation states were not determined. The XRF triplicates quantify within-sample analytical variability and do not establish reproducibility between independent reactions. VSM, magnetic separation, catalyst reuse, regeneration, and metal-leaching tests were not performed. Accordingly, magnetic recoverability, catalytic durability, and an exclusively heterogeneous reaction pathway are not established. The designation Fe_3O_4–kaolin refers to the formulation prepared using commercial Fe_3O_4 powder and does not substitute for magnetic characterization of the thermally treated composite.

4. Conclusions

Calcined and NaOH-modified Iranian kaolin served as a common support for Fe_3O_4–kaolin, Cu–kaolin, NiMo–kaolin, and CoMo–kaolin prepared by aqueous wet impregnation or dispersion-assisted deposition. XRD showed a disordered kaolin-derived background with residual mineral reflections and distinct crystalline contributions from the loaded metal systems. FTIR showed aluminosilicate framework vibrations with overlapping possible metal–oxygen contributions. SEM revealed different degrees of platelet preservation, granular coverage, and aggregation.

The comparison under common oxidation and extraction conditions identified Fe_3O_4–kaolin as the most effective formulation in the tested series. It reduced total sulfur from 1500 to 136 ppm, corresponding to 90.93% overall removal, compared with 44.00% for the metal-free support and 64.80, 63.00, and 48.67% for CoMo–kaolin, NiMo–kaolin, and Cu–kaolin, respectively. These efficiencies describe the combined oxidation–extraction procedure and establish the performance order under the reported conditions.

Acknowledgments

The authors would like to thank the reviewers and the Editor for their valuable contributions to enhancing the scientific quality of this research.

Author Contributions

All authors contributed equally to the conception, preparation, and writing of this manuscript.

Conflict of Interest

The authors, while observing publication ethics in the referencing, declare the absence of interest of conflict.

AI Use Statement

The author retains full responsibility for the accuracy, originality, integrity, legality, and ethical compliance of all text, data, tables, figures, analyses, references, and conclusions, and have verified all AI-assisted outputs. Any fabrication, falsification, manipulation, plagiarism, copyright infringement, or other misuse of AI remains solely the responsibility of the authors and does not transfer or diminish their accountability for the published work.

References

[1] Z. S. Mahmoudabadi, A. Rashidi, M. Yousefi, *Journal of Environmental Chemical Engineering*, 2021, **9(3)**, 1052001-11. https://doi.org/10.1016/j.jece.2021.105200

[2] B. Pouladi, M. A. Fanaei, G. Baghmisheh, *Journal of Cleaner Production*, 2019, **209**, 965-977. https://doi.org/10.1016/j.jclepro.2018.10.283

[3] A. Taghizadeh, M. Asemani, F. Esmaeilzadeh, A. Ameri, *ACS Omega*, 2023, **8(45)**, 42522-42539. https://doi.org/10.1021/acsomega.3c05193

[4] A. M. Dehkordi, Z. Kiaei, M. A. Sobati, *Fuel Processing Technology*, 2009, **90(3)**, 435-445. https://doi.org/10.1016/j.fuproc.2008.11.006

[5] M. A. Sobati, A. M. Dehkordi, M. Shahrokhi, *Fuel Processing Technology*, 2010, **91(11)**, 1386-1394. https://doi.org/10.1016/j.fuproc.2010.05.010

[6] C. Huang, P. Wu, Y. Guo, Y. Guo, *Microporous and Mesoporous Materials*, 2020, **306**, 1104151-7. https://doi.org/10.1016/j.micromeso.2020.110415

[7] H. M. Hmood, S. A. Gheni, S. M. R. Ahmed, M. M. Ali, H. Y. Saleh, M. H. Mohammed, A. E. Mohammed, M. A. Mahomood, H. R. Mohammed, A. A. Hassan, A. Harvey, *Particuology*, 2024, **84**, 249-260. https://doi.org/10.1016/j.partic.2023.06.016

[8] U. Arellano, J. M. Shen, J. A. Wang, M. T. Timko, L. F. Chen, J. T. Vázquez Rodríguez, M. Asomoza, A. Estrella, O. A. González Vargas, M. E. Llanos, *Fuel*, 2015, **149**, 15-25. https://doi.org/10.1016/j.fuel.2014.11.001

[9] L. Rivoira, J. Juárez, M. L. Martínez, A. Beltramone, *Catalysis Today*, 2020, **349**, 98-105. https://doi.org/10.1016/j.cattod.2018.05.030

[10] M. Ahmadian, M. Anbia, *Fuel*, 2022, **324**, 1244711-12. https://doi.org/10.1016/j.fuel.2022.124471

[11] X. An, L. Zhu, J. Xiao, W. Jiang, X. Gao, L. Xu, H. Li, W. Zhu, H. Li, *Fuel*, 2022, **325**, 1247551-8. https://doi.org/10.1016/j.fuel.2022.124755

[12] X. An, W. Jiang, L. Zhu, L. Xu, J. She, J. He, W. Zhu, H. Li, *Applied Catalysis B: Environment and Energy*, 2023, **333**, 1227791-12. https://doi.org/10.1016/j.apcatb.2023.122779

[13] ASTM International, *ASTM D4294-24: Standard test method for sulfur in petroleum and petroleum products by energy dispersive X-ray fluorescence spectrometry*, West Conshohocken, PA: ASTM International, 2024. doi:10.1520/D4294-24

[14] R. Javadli, A. de Klerk, *Applied Petrochemical Research*, 2012, **1(1-4)**, 3-19. https://doi.org/10.1007/s13203-012-0006-6

[15] A. Souri, F. Golestani-Fard, R. Naghizadeh, S. Veiseh, *Applied Clay Science*, 2015, **103**, 34-39. https://doi.org/10.1016/j.clay.2014.11.001

[16] Z. G. Asmare, B. A. Aragaw, M. Atlabachew, *ACS Omega*, 2024, **9(49)**, 48014-48031. https://doi.org/10.1021/acsomega.4c04029

[17] A. Magdy, Y. O. Fouad, M. H. Abdel-Aziz, A. H. Konsowa, *Journal of Industrial and Engineering Chemistry*, 2017, **56**, 299–311. https://doi.org/10.1016/j.jiec.2017.07.023

[18] S. Onutai, T. Osugi, T. Sone, *Materials*, 2023, **16(3)**, 9851-15. https://doi.org/10.3390/ma16030985

[19] C. Cui, Y. Dang, C. Luo, L. Wang, H. Peng, *Materials*, 2024, **17(2)**, 3671-18. https://doi.org/10.3390/ma17020367

[20] T. Aloui, N. Fourati, K. Khirouni, H. Guermazi, S. Guermazi, C. Zerrouki, *Measurement*, 2024, **236**, 1151711-10. https://doi.org/10.1016/j.measurement.2024.115171

[21] S. Sakthivel, S. Shobika, A. Dinesh, K. Yogalakshmi, R. Suriyaprakash, B. Kabilan, P. Sathyajith, S. Elumalai, L. Gnanasekaran, M. Ayyar, M. Santhamoorthy, *Results in Chemistry*, 2025, **13**, 1019561-9. https://doi.org/10.1016/j.rechem.2024.101956

[22] R. N. Dürr, P. Maltoni, S. Feng, S. Ghorai, P. Ström, C.-W. Tai, R. B. Araujo, T. Edvinsson, *Inorganic Chemistry*, 2024, **63(5)**, 2388-2400. https://doi.org/10.1021/acs.inorgchem.3c03261

[23] J. L. García-Gutiérrez, G. A. Fuentes, M. E. Hernández-Terán, P. García, F. Murrieta-Guevara, F. Jiménez-Cruz, *Applied Catalysis A: General*, 2008, **334(1-2)**, 366-373. https://doi.org/10.1016/j.apcata.2007.10.024

[24] Z. Lin, Z. Pan, Y. Zhao, L. Qian, , J. Shen, K. Xia, Y. Guo, Z. Qu, *Nanomaterials*, 2020, **10(7)**, 13701-23. https://doi.org/10.3390/nano10071370

[25] H. Mofid, M. R. Khosravi-Nikou, S. A. Razavi, M. Mohammadian, *Applied Thermal Engineering*, 2024, **245**, 1-17. https://doi.org/10.1016/j.applthermaleng.2024.122810

[26] S. A. Razavi, H. Motavali, *Journal of Industrial Engineering and Management Studies*, 2023, **10(2)**, 106-115. https://doi.org/10.22116/jiems.2023.399150.1516